Measuring Dynamics in Weakly Structured Regions of Proteins Using Microfluidics-Enabled Subsecond H/D Exchange Mass Spectrometry

ARTICLE *in* ANALYTICAL CHEMISTRY · APRIL 2012

Impact Factor: 5.64 · DOI: 10.1021/ac300365u · Source: PubMed

7 AUTHORS, INCLUDING:

Tamanna Rob
York University
7 PUBLICATIONS **124** CITATIONS
SEE PROFILE

Peter Liuni
York University
9 PUBLICATIONS **89** CITATIONS
SEE PROFILE

Derek J Wilson
York University
38 PUBLICATIONS **560** CITATIONS
SEE PROFILE

analytical chemistry

Article

pubs.acs.org/ac

Measuring Dynamics in Weakly Structured Regions of Proteins Using Microfluidics-Enabled Subsecond H/D Exchange Mass Spectrometry

Tamanna Rob,[†] Peter Liuni,[†] Preet Kamal Gill,[†] Shaolong Zhu,[†] Naresh Balachandran,[‡] Paul J. Berti,[‡] and Derek J. Wilson*[,†]

[†]Department of Chemistry, York University, Toronto, Ontario M3J 1P3, Canada

[‡]Department of Chemistry and Chemical Biology and Department of Biochemistry and Biomedical Sciences, McMaster University, Hamilton, Ontario L8S 4M1, Canada

Supporting Information

ABSTRACT: This work introduces an integrated microfluidic device for measuring rapid H/D exchange (HDX) in proteins. By monitoring backbone amide HDX on the millisecond to low second time scale, we are able to characterize conformational dynamics in weakly structured regions, such as loops and molten globule-like domains that are inaccessible in conventional HDX experiments. The device accommodates the entire MS-based HDX workflow on a single chip with residence times sufficiently small (*ca.* 8 s) that back-exchange is negligible (≤5%), even without cooling. Components include an adjustable position capillary mixer providing a variable-time labeling pulse, a static mixer for HDX quenching, a proteolytic microreactor for rapid protein digestion, and on-chip electrospray ionization (ESI). In the present work, we characterize device performance using three model systems, each illustrating a different application of 'time-resolved' HDX. Ubiquitin is used to illustrate a crude, high throughput structural analysis based on a single subsecond HDX time-point. In experiments using cytochrome *c*, we distinguish dynamic behavior in loops, establishing a link between flexibility and interactions with the heme prosthetic group. Finally, we localize an unusually high 'burst-phase' of HDX in the large tetrameric enzyme DAHP synthase to a 'molten globule-like' region surrounding the active site.

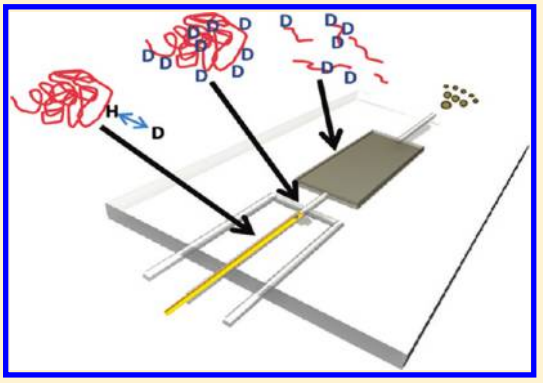

The tools of structural biology (*i.e.*, X-ray crystallography and structural NMR) provide an exquisitely detailed but largely static view of the physiologically relevant, 'native' structures of proteins.[1,2] The importance of these structures to understanding how proteins carry out their biological roles cannot be overstated, and yet if proteins were to adopt *only* the structures reported, many would be essentially nonfunctional.[3] Virtually all aspects of protein activity, from catalysis to ligand binding and allostery, depend on the ability to transiently adopt specific higher energy structures.[4−8] These 'excited states' are critical to function and can in some cases act as a gateway to misfolding and disease.[9−12] Thus, there is substantial motivation to understand not only the 'ensemble averaged' structures revealed by classical structural biology but also to characterize the transient, weakly populated structures that are adopted via conformational dynamics.

Excited protein states are challenging analytical targets because they are **i**) transient, **ii**) weakly populated at equilibrium, and **iii**) spectroscopically similar to the ground-state. In the early 1980s, backbone amide HDX was introduced as a means of measuring the integrity of hydrogen bonding networks in protein secondary structures, first by NMR[13] and later by mass spectrometry.[14] This approach is founded on the premise that solvent accessible backbone amide protons are protected from exchange with solvent if they are hydrogen bonded (as they are in secondary structures). The degree of protection reflects the strength of the hydrogen bond, and, averaging over adjacent amides, the stability of the secondary structure in question.[15]

In NMR experiments, HDX is usually measured as a time-dependent decrease in the volume of backbone amide proton HSQC cross-peaks.[13] NMR measurements are always site specific, but transverse relaxation limits conventional solution NMR experiments to proteins < ∼50 kDa, and acquisitions are typically on the minutes time scale, which severely limits the ability to monitor more dynamic regions.[16] In MS-based HDX experiments, exchange is monitored *via* the mass increase accompanying deuterium uptake. This approach is more amenable to time-resolved measurements and need not be size limited but usually provides 'segment averaged' HDX data.[17]

MS-based HDX methods can be divided into 'top-down' and 'bottom-up' approaches. Top-down experiments involve fragmentation of deuterium-labeled protein ions in the gas phase (i.e., postionization).[18] Top-down experiments can yield single-residue resolution, but the electron capture/transfer

Received: February 10, 2012
Accepted: March 29, 2012
Published: March 29, 2012

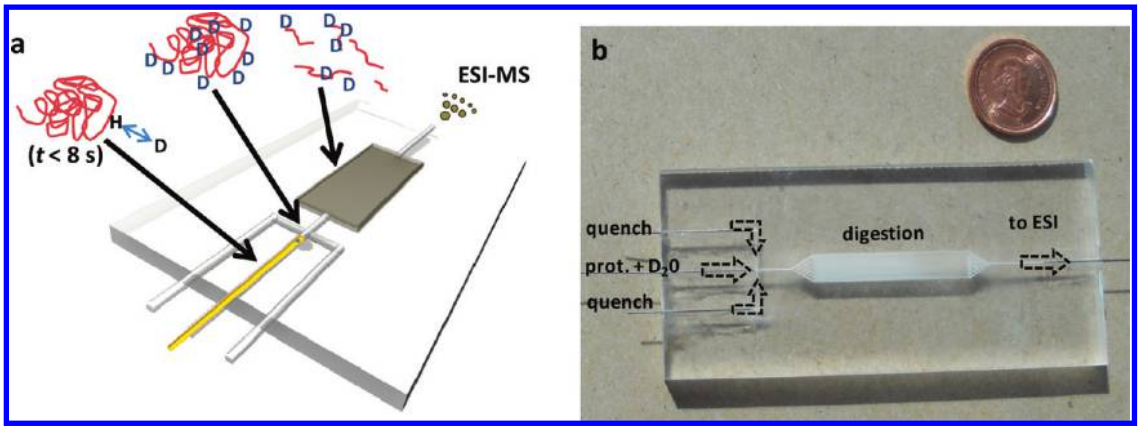

Figure 1. The microfluidic device. (a) A schematic depiction. Solutions are injected at the 'near' side of the device and ESI is carried out at the 'far' end. HDX is conducted under native conditions (pD 7.6) in the first phase with adjustable labeling times from ~40 ms to 8 s. This is followed by HDX quenching, which is achieved by dropping the pH to 2.5. The labeled protein is then injected into the proteolytic reactor, generating labeled peptides which can be located on the native structure. (b) A photograph of the device, with coin for scale.

fragmentation methods that are used (to avoid 'scrambling')[19−21] require more specialized equipment and impose an effective size limit[5] due in part to decreasing fragmentation efficiency with increasing size. The 'bottom-up' approach involves quenching of the HDX reaction by acidification, followed by proteolytic digestion using an acid-resistant protease.[14] In this case, spatial resolution is a function of digestion efficiency and typically ranges from 4 to 10 residues.[22] Thus, bottom-up HDX experiments yield 'segment averaged' data which are semiquantitative. The advantage of the bottom-up approach is that it is broadly applicable; there is no inherent size limit and it can be carried out using widely available, nonspecialized instrumentation.

One of the challenges of implementing bottom-up HDX is the occurrence of back-exchange during the proteolytic and LC steps, which are carried out in H_2O. Back-exchange not only dampens the structural information acquired during forward-labeling, it also does so in a site-specific manner that is governed more-or-less exclusively by the primary sequence (in contrast to the forward-exchange step, which is also structure dependent).[23] Thus, significant back-exchange can lead to an artifactual deuteration 'profile' that is more reflective of the intrinsic back-exchange rates than conformational dynamics. Back-exchange can usually be kept to manageable levels by lowering the solvent pH to ~2.5 and the temperature to 0 °C, but sacrifices to digestion and/or separation efficiency are frequently made to avoid lengthy on-column times.[24]

In a typical backbone-amide HDX experiment, exchange is measured over a period of minutes-to-hours.[22,25,26] This time scale is appropriate for structured region of the protein because, while dynamics and the accompanying fluctuations between a hydrogen bonded 'closed' state and an unbonded 'open' state may be rapid, the equilibrium K_{op} will strongly favor the 'closed' state, greatly slowing the observed rate of exchange. In more dynamic regions such as loops and weak secondary structures, however, conventional HDX measurements yield only a 'burst-phase' of exchange which, especially in loops, is commonly 100%. This limitation is unfortunate given the critical role that dynamic regions often play in protein function, and the biological importance of 'intrinsically disordered' proteins, which are largely dynamic in their native state.

In this work, we introduce a microfluidic device that enables time-resolved (*i.e.*, millisecond time-scale) MS-based HDX measurements, integrating all of the necessary components for a bottom-up workflow with online ESI. This approach provides a powerful alternative to quench-flow experiments,[27,28] which are limited by decoupled sample handling and analysis and CLEANEX NMR,[29,30] which shares size and time-scale restrictions with other NMR methods. Residence times in the device are small relative to other techniques, ensuring minimal back-exchange. Our present aim is to characterize device performance and to illustrate the utility of time-resolved HDX experiments. Three model systems are investigated including a single time-point structural analysis of ubiquitin, a comparison of loop dynamics in cytochrome *c*, and a localization of conformational flexibility in the substrate-free form of a large tetrameric enzyme, DAHP synthase.

EXPERIMENTAL SECTION

Materials. Horse heart cytochrome *c*, ubiquitin, pepsin, deuterium oxide (D_2O), ammonium hydroxide, ammonium acetate (99.8%), 2-propanol (70% in water), and high purity acetic acid (≥99.7%) were purchased from Sigma (St. Louis, MO). Polyimide coated glass capillaries (O.D. 153 μm, I.D. 75 μm) were supplied by Polymicro Technologies (Pheonix, AZ). Metal capillaries (O.D. 400 μm, I.D. 200 μm and O.D. 318 μm, I.D. 158.75 μm) were purchased from Small Parts, Inc. (Miramar, FL). PTFE tubings (O.D. 1/16″, I.D. 400 μm and O.D. 1/16″, I.D. 205 μm) were supplied by McMaster Plastics (Scarborough, ON). Standard 1/16″ fittings were purchased from Upchurch (Oak Harbor, WA). Ultrapure water was generated in-house on a Millipore Milli-Q Advantage A10 system. The rotary grinder (Craftsman Co. Hoffman Estates, IL) was used to sharpen the metal capillary.

Microfluidic Device Fabrication. The multistep microreactor is an integration of a rapid mixing module[31] and a rapid proteolysis module[32] that were developed earlier. The device was fabricated on blank poly(methyl methacrylate) or PMMA substrate which was purchased from Professional Plastics (Fullerton, CA) in rectangular block with dimension of 8.9 cm × 3.8 cm × 0.3 cm. The microfluidic channels and well (32 mm × 5 mm × 0.01 mm) were etched on PMMA using a LASER engraver (Universal Laser, Scottsdale, AZ) following the protocol described by Rob et al.[31] The concentric capillary mixer was incorporated in the central channel of the device using a soldering iron. Two additional metal capillaries were

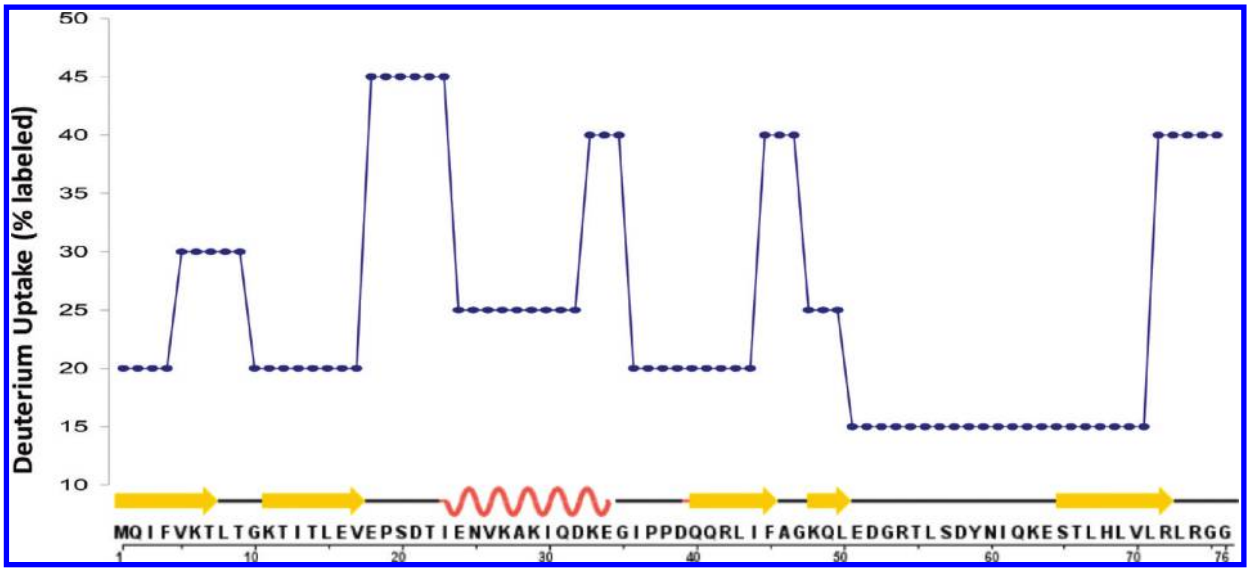

Figure 2. A crude secondary structure analysis of Ubiquitin using a single, subsecond HDX time-point (100 ms). The *y*-axis corresponds to deuterium uptake in '% deuterated', while the *x*-axis represents the primary sequence from the N-terminus on the left. Exchange levels of overlapping peptides are averaged, and the small 'uncovered' regions are assumed to be an average of the two flanking exchange levels.

similarly incorporated into adjacent channels to support connections to infusion pumps (Harvard, Holliston, MA) using standard Upchurch fittings. A closed polyimide-coated glass capillary was used as a static mixer to ensure efficient mixing of acid and deuterated protein before the quenched solution was transferred to proteolytic module. Pepsin was covalently attached to the floor and ceiling of the reactor well using protocol described by Brown et al.[33] Parafilm was used as gasket to obtain liquid-tight seal between the two activated PMMA blocks. A custom built clamp was obtained from LAC Machine & Tooling Limited, ON to pressure-seal the microfluidic device.[32]

DAHP Synthase (Phe) Purification. *Escherichia coli* Phe-regulated DAHP synthase (aroG) was produced in *E. coli* BL21*(DE3) cells harboring a pET300/*aroG* plasmid which contained *aroG* with an *N*-terminal TEV-protease-cleavable His_6-tag. Details on protein expression and purification are provided in the Supporting Information.

H/D Exchange Measurements. HDX studies were carried out with ubiquitin, cytochrome *c*, and DAHP synthase using the integrated microfluidic chip as a custom electrospray ionization (ESI) source (Figure 1). The chip was directly interfaced with a modified QSTAR Elite hybrid quadrupole time-of-flight (QqTOF) mass spectrometer (Sciex, MDS Analytical Technologies, Concord, ON). The instrument was operated in positive ion mode with source voltage +4800 V. ESI was performed at room temperature without source assembly heating and with a collateral flow of dry nitrogen to assist in desolvation. Moderate declustering conditions (declusturing potential = 60−90 V, focusing potential = 200−250 V) were chosen to minimize in-source heating.

50 μM ubiquitin, 500 μM cytochrome *c*, and 270 μM DAHP synthase were mixed with D_2O (1:3) in the rapid mixing module of the device (pD 7.6). The position of the mixer in the mixing module was adjusted manually to control the labeling time. Using flow rates of 1 μL/min for protein solution and 3 μL/min for D_2O we were able to achieve labeling times from 42 ms to 10 s. Labeling was rapidly quenched by dropping the solution to pH 2.6 by using a 4% acetic acid solution (pH 2.3) at 9 μL/min (2 × 4.5 μL/min). Digestion and electrospray was therefore ultimately carried out in a 77:23 H_2O/D_2O mixture. Digestion of deuterated proteins and transfer to the ESI emitter was carried out in approximately 8 s to minimize the back-exchange of backbone amides (protons on side chain and termini were assumed to be fully equilibrated with the electrosprayed solution prior to ionization).

Peptide exchange levels were modeled using a custom built FORTRAN program, based on an analytical framework described previously,[19] with 'offset' adjustments for backbone amide back-exchange (determined using the neuropeptide bradykinin as an internal standard, always ≤5%) and equilibrated exchange at side-chains and termini.

Data Analysis. Details of the data analysis method are provided in the Supporting Information. Briefly, time-resolved HDX data differ from those collected in conventional experiments in that the time-scale is sufficiently short that we expect essentially no contribution from amides in secondary structures. In cases where we can define the position of loop amides based on a reported X-ray or NMR structure, we compare the amplitude of the observed exchange N_{fast} to the number of loop backbone amides N_{loop}. If N_{fast} and N_{loop} are in reasonable agreement in a given segment, then it is likely that the reported structure reflects the solution conformation under our conditions, and we attribute the observed exchange specifically to loop amides. The condition $N_{fast} \ll N_{loop}$ suggests that the loop reported in the structure is extensively hydrogen bonded and may include unreported secondary structure. Conversely, when $N_{fast} \gg N_{loop}$, this would indicate that a reported secondary structure element is weakly populated (or possibly not even present) under our conditions.

The observed HDX kinetics profiles are fit to a modified single exponential expression as described in the Supporting Information. From this fit, we extract the segment averaged rate of exchange k_{ex}. Protection factors (PFs) are defined as k_{int}/k_{ex} where k_{int} is the average intrinsic rate of exchange for the segment. If $N_{fast} \approx N_{loop}$, the average intrinsic rate k_{int} is calculated specifically from loop amides.

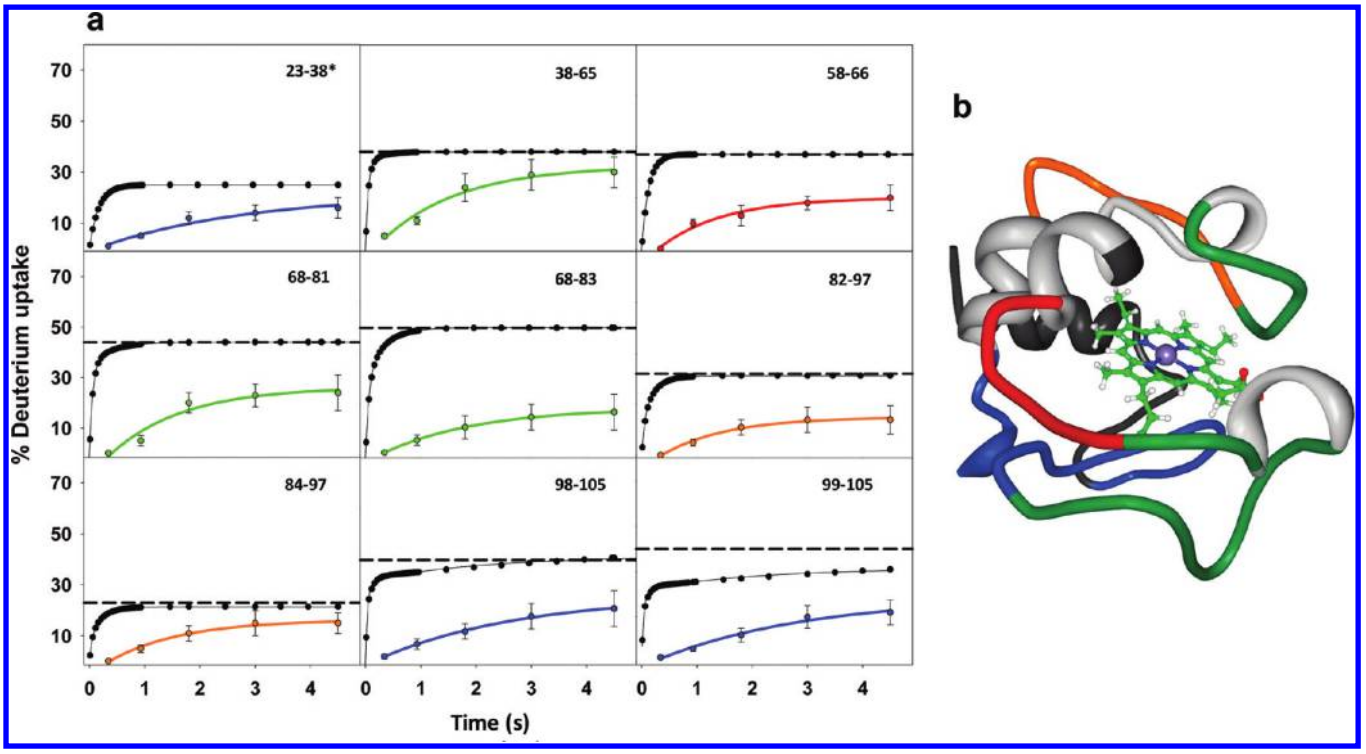

Figure 3. (a) Representative kinetic plots of '% exchanged' vs time for 9 peptides from cytochrome *c*. The 'loop amide only' profiles based on the intrinsic rates $D(t)_{int}$ are shown in black. The dashed line represents 100% exchange of loop amides (*i.e.*, N_{loop}). The measured profiles are colored by PF; blue (strong protection), green (moderate protection), orange (low protection), red (very low protection). For segment 23−38, marked with (*), N_{fast} (27% ± 5) is not comparable to N_{loop} (100%). The intrinsic profile for that segment was therefore constructed from the lowest 5 (*i.e.*, 30% of 15 amides) intrinsic rates, which gives the 'lower bound' PF of 16. Error bars are from two or three replicates depending on the number of experiments in which the peptide was detected. (b) Cytochrome *c* loop dynamics based on time-resolved HDX data. Differing levels of protection in loops are mapped onto the solution structure for oxidized horse heart cytochrome *c* (1AKK)[46] by PF: blue (strong protection), green (moderate protection), orange (weak protection), red (very low protection). Structured regions covered by observed peptides are shown in light gray. Regions for which no peptides were observed are colored dark gray. Image generated using Protein Workshop.[50]

RESULTS AND DICUSSION

Microfluidics. The integrated microfluidic device for time-resolved HDX experiments is shown in Figure 1. PMMA was selected as the substrate to allow straightforward fabrication *via* laser ablation;[31] however, this introduced a risk of sample contamination due to dissolution of PMMA, particularly in the acid quench solution channel. Fortunately, blank control experiments showed no signs of PMMA degradation, which we have observed previously as the appearance of a polydisperse PMMA polymer signal in the range of 300−1500 *m/z*. In earlier iterations of our proteolytic reactor, we used pepsin-agarose beads which were attached to the floor of the reactor well *via* adhesion.[32,34] The activity of these reactors was sufficient, but the continuous-use lifetime was limited to *ca.* 8 h. In this study, we used a covalent attachment protocol developed by Brown and co-workers[33,35] which decreased digestion efficiency slightly but improved the continuous-use lifetime to more than 56 h.

To facilitate HDX experiments, our primary design objective was to maintain efficient protein digestion while minimizing back-exchange which, in practice, meant optimizing the geometry of the proteolytic reactor well. We found ultimately that a well with dimensions length = 32 mm, width = 5 mm, and depth = 10 μm (vol. = 1.6 μL) provided sufficient digestion while keeping back-exchange sufficiently low as to have a negligible impact on the data.[36] While always ≤5%, back exchange was highly variable run-to-run, suggesting that it may have been arisen from ESI source conditions.[37] At the flow rates used, the reactor well and transfer volumes correspond to a total postquench residence time of approximately 8 s. An analysis of the dependence of sequence coverage and peptide length on well geometry is provided in the Supporting Information (Table S1). Using the geometry given above,

Table 1. Time-Resolved HDX Parameters for Peptides from Cytochrome *c*

segment	N_{loop} (% of peptide)	N_{fast} (% of peptide)[a]	PF
23−38	100	27 ± 5	57 ± 12[b]
38−65	38	41 ± 6	12 ± 3
58−66	37	31 ± 4	5 ± 1
68−81	44	40 ± 6	10 ± 3
82−97	33	25 ± 6	6 ± 3
84−97	23	26 ± 7	8 ± 4
84−95	30	32 ± 8	12 ± 5
96−105	33	27 ± 6	22 ± 6
98−105	40	32 ± 4	25 ± 5
99−105	47	36 ± 8	27 ± 8

[a]Error measurements are based on two or three replicates depending on the number of experiments in which the peptide was detected. [b]Since $N_{fast} \ll N_{loop}$ for this peptide, we can provide only an estimate of the PF based on the average intrinsic rate for the whole peptide. We can also determine upper and lower bounds by assuming that the amides contributing to the observed exchange are those with the lowest and highest intrinsic rates, respectively.

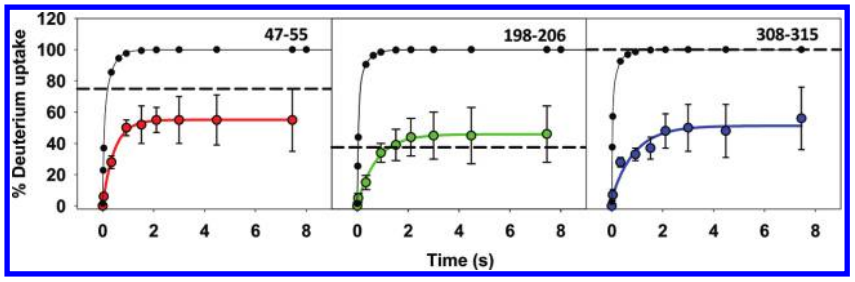

Figure 4. HDX kinetics for representative peptides from DAHP synthase. Intrinsic rate profiles $D(t)_{int}$ for each segment are shown in black. The measured profiles are represented by filled circles colored according to the extracted PF: blue (strong protection), green (moderate protection), red (low protection). For most peptides, there is little correlation between N_{fast} and the number of loop amides in the substrate-bound structure.

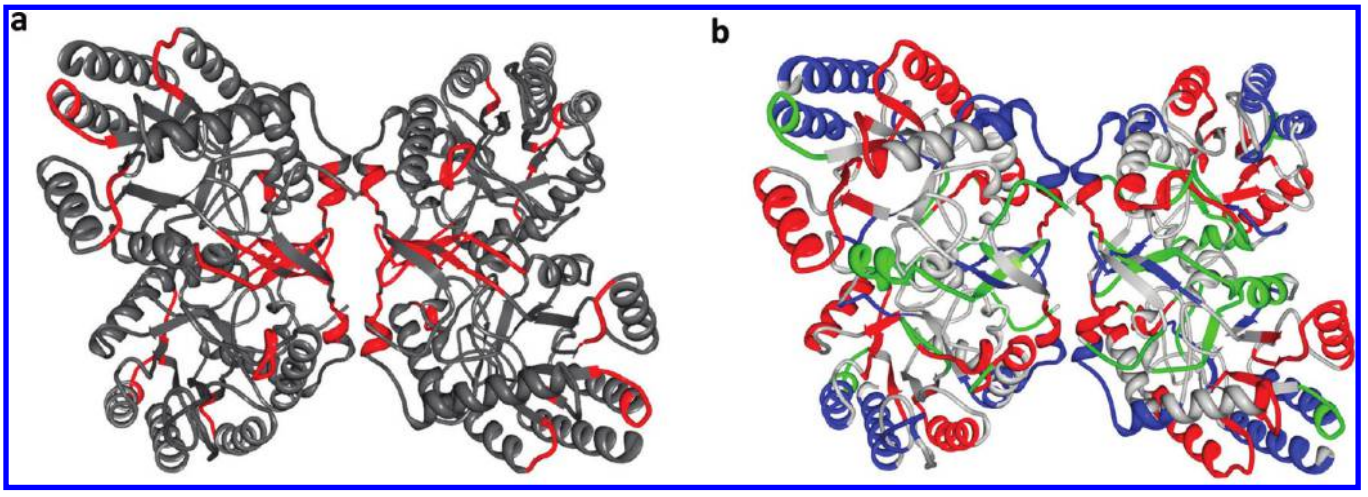

Figure 5. DAHP exchange profiles mapped on to the substrate-bound 1KFL structure. (a) Highlighted regions correspond to peptides in which N_{fast} is in reasonable agreement with N_{loop}, suggesting similarity between the apoprotein structure and the PEP-bound structure (1KFL).[48] Many of the peptides with this property are located at the tetramer interface. (b) Observed peptides are mapped onto the PEP-bound DAHP structure (1KFL), colored by PF: blue (strong protection), green (moderate protection), red (low protection). Note that on our relative scale even 'strong protection' corresponds to looplike exchange (PF $\leq$ 32), thus many regions that are structured in the substrate-bound state (N_{loop} = 0) are clearly much less so in the apoprotein ($N_{fast} \gg N_{loop}$). Images were created using Protein Workshop.[50]

and activating both the 'floor' and the 'ceiling' of the reactor, sequence coverage was 85% for ubiquitin, 60% for cytochrome *c*, and 60% for DAHP synthase with an average peptide length of 5 a.a. (ubiquitin), 9 a.a. (cytochrome *c*), and 6 a.a. (DAHP synthase). These statistics translate into sufficient spatial resolution to provide meaningful measurements of local conformational dynamics, but as always in bottom-up experiments, enhancement of digestion efficiency (without increasing residence times) is an avenue for further development.

The adjustable capillary mixing component, which is adapted from a mixer introduced by Wilson and Konermann,[38] allowed HDX labeling times between roughly 40 ms and 8 s. We used the mixer in static mode, meaning that the mixer is held at a fixed position to allow for indefinite time acquisitions at a single reaction time-point. This was mainly to allow for complete flushing of old material from the proteolytic reactor prior to the initiation of measurements at a new time increment. We found that flushing for 5 min after adjusting the capillary position to the new time-point was sufficient to prevent carryover of old material, based on stabilization of the exchange level for all peptides.

Single Time-Point Structural Measurements. One of the most straightforward applications of spatially resolved HDX measurements is a crude (but high throughput) structural analysis based on a single time-point measurement.[5,39] These experiments rely on the substantial difference between K_{op} in structured and unstructured regions to determine the locations of secondary structures. The approach is feasible because k_{int} is distributed over a much narrower range (around 2 orders of magnitude) than K_{op}; thus amides with high intrinsic rates in structured regions will still exchange much more slowly than amides with low intrinsic rates in unstructured regions. A single time-point spatially resolved HDX profile should therefore reflect the locations of secondary structure elements (and to a lesser extent, solvent accessibility).[22] As labeling time increases, however, amides with progressively lower K_{op} begin to acquire a significant amount of label and the 'secondary structure map' begins to blur. Thus, the optimal labeling time is one that is sufficiently long to minimize contributions from the segment averaged k_{int} and sufficiently short to maximize the contrast between structured and unstructured regions. At physiological pH, this would correspond to a subsecond labeling time on the order of 100 ms.

To demonstrate the acquisition of a secondary structure map using our apparatus, we have acquired a single time-point (100 ms) HDX profile for ubiquitin (Figure 2). In general, the profile agrees with the known structure of ubiquitin, with α-helices and β-strands exhibiting a substantially lower deuterium uptake than loops. One interesting feature is that even the most highly labeled loops underwent only 50% of their potential deuterium uptake, whereas, based on k_{int} alone, most should be essentially 100% labeled. This would suggest that amides

Table 2. Time-Resolved HDX Statistics for Peptides from DAHP Synthase

segment	N_{loop} (% of peptide)	N_{fast} (% of peptide)[a]	PF
3–9	100	57 ± 10	16 ± 6
18–23	50	59 ± 12[b]	5 ± 4
24–36	17	100 ± 5	27 ± 6
47–55	75	55 ± 10	6 ± 3
69–72	0	48 ± 11	5 ± 3
83–88	100	97 ± 9[b]	2 ± 1
88–91	0	69 ± 12	2 ± 1
96–108	77	100 ± 11	11 ± 3
97–102	80	100 ± 17	10 ± 4
105–113	25	61 ± 8	6 ± 2
108–114	50	92 ± 10	5 ± 3
108–117	67	74 ± 12[b]	15 ± 5
118–123	0	73 ± 10	9 ± 3
118–124	0	77 ± 15	8 ± 4
134–140	33	98 ± 19	23 ± 9
158–165	57	73 ± 11	15 ± 5
186–191	100	68 ± 14	24 ± 8
196–203	0	76 ± 16	11 ± 6
198–206	38	45 ± 9[b]	12 ± 3
205–216	55	64 ± 10[b]	14 ± 4
216–220	50	54 ± 7[b]	24 ± 5
222–226	50	50 ± 6[b]	32 ± 5
232–235	33	98 ± 16	4 ± 1
250–253	0	75 ± 18	7 ± 3
254–257	33	73 ± 16	9 ± 4
258–262	75	73 ± 12[b]	5 ± 2
262–267	40	55 ± 10	3 ± 1
262–268	50	68 ± 10	5 ± 2
276–281	0	18 ± 5	25 ± 11
282–293	18	74 ± 13	20 ± 6
284–293	22	62 ± 9	12 ± 3
289–294	60	59 ± 8[b]	12 ± 2
290–296	83	87 ± 17[b]	16 ± 4
292–296	100	72 ± 15	11 ± 3
300–305	100	74 ± 11	8 ± 2
308–315	100	47 ± 18	23 ± 11
309–313	100	60 ± 15	32 ± 8
343–346	0	50 ± 12	19 ± 9

[a]Error measurements are based on two or three replicates depending on the number of experiments in which the peptide was detected. [b]Indicates peptides where there is a reasonable correlation (≤10% difference) between N_{loop} and N_{fast}. PFs for these peptides were generated using 'loop localized' intrinsic rate profiles. The positions of these peptides in the substrate-bound structure (1KFL) are shown in Figure 5a.

located in loops still have substantial attenuation of k_{int} by K_{op}, a finding that is corroborated by NMR CLEANEX measurements which typically show loop K_{op} values between 1 and 0.1.[30] There was also low-level labeling (up to 20%) in regions of secondary structure. This can be attributed somewhat to averaging of exchange levels in overlapping segments, but mostly it results from the fact that not all amides in secondary structure elements are hydrogen bonded (e.g., the N-termini of α-helices and the outward-facing side of edge β-strands).

There are some regions where the profile is not as expected, most notably the large loop preceding the C-terminal β-strand (the $\beta4-\beta5$ loop) where low HDX uptake suggests substantially more protection than would be expected in a loop. In fact, this observation is supported by NMR-based measurements including extended time scale order parameters which indicate a relatively low degree of conformational flexibility in this loop on the μs time scale.[40] NMR HDX measurements also show an intermediate degree of protection (i.e., substantially more than a typical loop, but less than a secondary structure) in this region.[41] The X-ray structure (PDB code 1UBQ)[42] suggests that this increased protection may stem from extensive hydrogen bonding of the $\beta4-\beta5$ loop amides with residues in the N-terminus of $\alpha1$-helix and the $\beta5$-strand.

Taken together, our ubiquitin data illustrate both the advantages and disadvantages of using ms time scale deuterium pulses for secondary structure profiles. The contrast between secondary structures and loops (where they are detected) is very high, but the short labeling time results in an oversensitivity to intermediate degrees of protection (*e.g.*, in the $\beta4-\beta5$ loop) which can lead to 'false positives' for secondary structure. On the other hand, these single time-point 'false positives' hint at the primary advantage of short labeling time HDX kinetics, namely the ability to distinguish very low protection from low-moderate protection in weakly structured regions.

Characterizing Conformational Dynamics in Weakly Structured Regions. We used loop dynamics in native cytochrome *c* to illustrate the ability to characterize dynamics in weakly structured regions at physiological pH. Cytochrome *c* is not an ideal candidate for our approach in that it is a poor substrate for pepsin;[43] however, its native state conformational dynamics have been extensively characterized, providing the best option for a methodological comparison.[44,45] Sequence coverage was 60% overall, with 100% coverage in the C-terminal half of the protein but no peptides detected from the N-terminal region. Some of this lack of coverage at the N-terminus may stem from the presence of covalently bound heme (Cys 14 and Cys 17), which would likely have had a deleterious effect on pepsin activity.

To accurately characterize conformational dynamics, it is necessary to monitor deuterium uptake as a function of time, *i.e.*, HDX kinetics. Typical raw data that contribute to the kinetic profiles for 3 peptides are shown in the Supporting Information (Figure S1). The '% exchanged' value for each time-point is determined by fitting the observed isotopic distribution to a theoretical one generated using a custom FORTRAN program (black circles) with adjustment to account for various labeling offsets caused by the composition of the exchange solution and equilibrated HDX on side-chains and termini (see data analysis section). We observe a continuous mass increase as a function of time indicating that exchange is in the EX2 regime, which is typical under native conditions.

To analyze the HDX kinetics, we plot '% exchanged' vs. time (Figure 3a), which corresponds to $D(t)$ as discussed in the data analysis section. HDX kinetics plots for 9 representative cytochrome *c* peptides together with the 'loop localized' intrinsic rate profiles $D(t)_{int}$. The observed profiles are colored by PF from blue (high protection) to red (very low protection). A graphical summary of the cytochrome *c* results (Figure 3b) shows the observed peptides mapped onto the solution structure of horse heart cytochrome *c* (PDB code 1AKK)[46] and colored according to the PF from blue (high protection) to red (very low protection). These PFs are derived exclusively from short labeling pulse HDX measurements, corresponding to exchange processes that are essentially complete after 4.5 s. On this time scale, there should be virtually no contribution from regions with secondary structure, an assumption that can

be tested by comparing the amplitude of the observed exchange to the amount of secondary structure in the peptide. For example, the peptide corresponding to residues 84−95 is 30% loop in the native structure. The amplitude for the 'fast' exchange component N_{fast} is 32 ± 8%, which agrees very closely with the expected contribution from loop amides. We observe a similar correlation for almost all peptides, which indicates a good agreement between the NMR structure and the actual structure of the protein in solution and supports the assumption that the observed exchange is attributable specifically to loop amides. Coloring is therefore restricted to loops (Figure 3b), and average k_{int} values for PF calculations are derived from loop amides only. In the instance where N_{fast} is substantially lower than the number of loop amides (*i.e.* segment 22−37), the whole peptide is shown colored and the PF was estimated using the average k_{int} for the whole segment. N_{loop} and N_{fast} values for each peptide are provided in Table 1, together with 'loop localized, segment averaged' PFs.

From the HDX kinetics measurements overall, it is clear that the loops in cytochrome *c* have substantially different dynamic properties, with 'segment averaged' PFs ranging from 5 ± 1 (α2−α3 loop) to 57 ± 12 (the α1−α2 loop). While there are to the best of our knowledge no directly comparable measurements of native cytochrome *c* loop dynamics under native conditions, our profile is generally in good agreement with 'native state HDX' thermodynamic stability measurements by Englander and co-workers[44,45] and can be rationalized by focusing on the influence of the heme prosthetic group. For instance, the least dynamic loop segment (22−37) is from the same loop as the heme covalent attachment site (Cys 14 and Cys 17) and is likely rigidly held in place by interactions between heme and its binding pocket. This loop is identified in native HDX experiments as being particularly resistant to denaturation.[44,47] In fact, many backbone amides in the 22−37 segment are so strongly hydrogen bonded that exchange is only at 40% after 48 h of incubation in D_2O (data not shown). Since on our rapid time-scale measurements detected exchange in only 5 of the amides from this 15 residue peptide (N_{fast} = 27 ± 5%, N_{loop} = 100%), the upper and lower bounds on the PF are widely separated. Taking the slowest 5 intrinsic rates, the PF would be 16, corresponding to the second-highest protection factor bin (green). If we assume that amides contributing to the observed exchange are those with the 5 fastest k_{int}, the PF is 102, corresponding to the highest protection factor bin (blue). In either case, it appears all amides in the α1−α2 loop are substantially protected.

The most rapid exchange was measured in the α2−α3 loop (PF = 5 ± 1) which has only one significant contact with heme (a hydrogen bond between a heme carboxylate and the Trp59 ε^1N proton). The α4−α5 loop showed a dual dynamic character, with significant protection near the α4 helix where there are substantial contacts with heme (including Met80 which is an axial ligand for the heme iron), and lower protection as the loop moves away from the heme binding pocket approaching the α5 helix. At pD 7.6, all of the exchange processes that allow us to compare loop dynamics are complete within a few seconds of initiating exchange. The time-resolution afforded by our apparatus is therefore crucial to the acquisition of loop dynamics profiles of this type.

Localizing Dynamics in a Large Tetrameric Enzyme. The primary advantage of bottom-up HDX is that it is a *general* method. It is applicable to virtually any protein and is not size-limited. Here we demonstrate a time-resolved, bottom-up HDX analysis on the enzyme DAHP synthase, a 154 kDa homotetramer. Our interest in DAHP synthase stems from 'global' HDX measurements (*i.e.*, no digestion prior to analysis) in which it was observed that, in the absence of substrate, the protein underwent a very large (∼65%) burst-phase of backbone amide exchange within 20 s of D_2O exposure, suggesting an unusually high degree of conformational flexibility in the unbound tetramer. The substrate-bound protein, on the other hand, showed a more typical ∼25% burst-phase (data not shown). This was consistent with efforts to crystallize the protein, which were successful only in the presence of substrates (or competitive inhibitors).[48] In this section, we use our microfluidic device to localize and characterize this burst-phase exchange.

Typical kinetic profiles from three DAHP peptides (Figure 4) illustrate the major difference between DAHP exchange kinetics and those from cytochrome *c*, which was that the majority of DAHP peptides showed no correlation between N_{fast} and N_{loop} values. N_{loop} was determined from the available substrate-bound structure (PDB code 1KFL).[48] For example, the peptide 118−124 is 100% α-helix in the 1KFL structure, and yet we still detect a large number of backbone amides undergoing exchange (N_{fast} = 77 ± 15%) with low protection. This would suggest that the 118−124 α-helix is at most weakly structured in the absence of substrate. The general lack of correlation between N_{fast} and N_{loop} in our DAHP data indicates substantial structural and/or dynamic differences between the substrate-bound and unbound forms of the protein (which is expected based on the 'global' HDX results). Nonetheless, electrospray mass spectra of DAHP strongly suggested that the protein was able to retain its native tetrameric configuration in the absence of substrate (data not shown). In fact, the HDX data are consistent with this observation in that those peptides that *do* show a good correlation between N_{fast} and N_{loop} are concentrated at the tetramer interface (Figure 5a). Thus, we can infer that the tetramer interface structure reported in 1KFL is largely intact in the unbound protein.

A second general difference from the cytochrome *c* data is that the overall level of exchange is much higher, averaging 73% (average exchange level for cytochrome *c* = 30%). This is consistent with a weak hydrogen bonding network undergoing 'molten globule-like' dynamics over a significant fraction of the protein.[49] Characterizing this weak network is important, since it may represent a template for the rapid development of structure upon substrate binding. 'Segment averaged' PFs, N_{fast} amplitudes, and N_{loop} for each DAHP peptide are provided in Table 2.

The DAHP synthase dynamics profile is mapped onto the substrate-bound structure 1KFL (Figure 5b) with observed peptides colored by PF from blue (high protection) to red (very low protection). Based on the profile, it is evident that the large burst-phase of exchange is localized to an area surrounding the active site, where all peptides underwent substantial exchange independent of their structural content in 1KFL. All of these segments are well positioned to be strongly influenced by the presence of substrate in the active site. Least protected was the region corresponding to the α3-helix (PF = 7 ± 3). Two helices located at the center of the group of α-helices surrounding the active site (α11 and α10) had a significant level of protection (PF 27 ± 8 and 20 ± 6) in the unbound protein, suggesting the presence of 'residual' structure. These regions and others with significant 'residual' structure in the unbound-protein (blue color, Figure 5b) may represent

nuclei for the rapid development of structure upon substrate binding.

CONCLUSIONS

We have demonstrated a new, broadly applicable approach for measuring dynamics in weakly structured regions of proteins. The method represents a powerful tool for characterizing dynamics in loops, molten-globules, and other weakly structured elements that are inaccessible in conventional experiments at physiological pH. By incorporating the entire HDX experimental workflow onto a single microfluidic chip, and using short (ms to s) labeling times, we were able to (**i**) produce high contrast secondary structure predictions using single time-point measurements, (**ii**) differentiate the dynamic properties of loops, and (**iii**) characterize weak hydrogen bonding networks in 'molten globule-like' protein segments. These experiments are straightforward and inexpensive and have a wide range of applications in ligand binding, protein aggregation/amyloidosis. The method provides a versatile platform to enhance our understanding of dynamics in weakly structured regions and may offer much-needed insights into the structural properties of 'intrinsically disordered' proteins.

ASSOCIATED CONTENT

Supporting Information

Details of protein expression/purification procedures. Development of data analysis method for short time-scale HDX measurements. Details of effects of reactor well size on sequence coverage and peptide length (Table S1). Raw HDX data for 3 cytochrome *c* peptides with isotope fits to the isotopic distributions (Figure S1). This material is available free of charge via the Internet at http://pubs.acs.org.

AUTHOR INFORMATION

Corresponding Author

*Phone: +1 416-736-2100 x20786. E-mail: dkwilson@yorku.ca.

Notes

The authors declare no competing financial interest.

ACKNOWLEDGMENTS

We thank Dr. Lars Konermann for helpful discussions. This work was supported by the Natural Sciences and Engineering Council of Canada (NSERC) Discovery Grant program, the Ontario Ministry of Research and Innovation Early Researcher Award, an Alzheimer's Society of Canada Biochemical Research Grant, and an operating grant from the Canadian Institutes of Health Research (MOP-64422).

REFERENCES

(1) Kresten Lindorff-Larsen, R. B. B.; DePristo, M. A.; Dobson, C. M.; Michele, V. *Nature* **2005**, *433*, 128−132.
(2) Frauenfelder, H.; Sligar, S. G.; Wolynes, P. G. *Science* **1991**, *254*, 1598−1603.
(3) Sterner, R.; Liebl, W. *Crit. Rev. Biochem. Mol. Biol.* **2001**, *36*, 39−106.
(4) Benkovic, S. J.; Hammes-Schiffer, S. *Science* **2003**, *301*, 1196−1202.
(5) Pan, J. X.; Han, J.; Borchers, C. H.; Konermann, L. *J. Am. Chem. Soc.* **2009**, *131*, 12801−12808.
(6) Mulder, F. A. A.; M., A.; Hon, B.; Dahlquist, F. W.; Kay, L. E. *Nat. Struct. Mol. Biol.* **2001**, *8*, 932−935.
(7) Eisenmesser, E. Z.; Millet, O.; Labeikovsky, W.; Korzhnev, D. M.; Wolf-Watz, M.; Bosco, D. A.; Skalicky, J. J.; Kay, L. E.; Kern, D. *Nature* **2005**, *438*, 117−121.
(8) Kern, D.; Zuiderwegy, E. R. P. *Curr. Opin. Struct. Biol.* **2003**, *13*, 748−757.
(9) Hartl, F. U.; Hayer-Hartl, M. *Nat. Struct. Mol. Biol.* **2009**, *16*, 574−581.
(10) Bemporad, F.; Calloni, G.; Campioni, S.; Plakoutsi, G.; Taddei, N.; Chiti, F. *Acc. Chem. Res.* **2006**, *39*, 620−627.
(11) Bucciantini, M.; Giannoni, E.; Chiti, F.; Baroni, F.; Formigli, L.; Zurdo, J. S.; Taddei, N.; Ramponi, G.; Dobson, C. M.; Stefani, M. *Nature* **2002**, *416*, 507−511.
(12) Sanchez-Ruiz, J. M. *Biophys. Chem.* **2010**, *148*, 1−15.
(13) Wagner, G.; Wuthrich, K. *J. Mol. Biol.* **1982**, *160*, 343−361.
(14) Zhang, Z. Q.; Smith, D. L. *Protein Sci.* **1993**, *2*, 522−531.
(15) Englander, S. W.; Sosnick, T. R.; Englander, J. J.; Mayne, L. *Curr. Opin. Struct. Biol.* **1996**, *6*, 18−23.
(16) Mori, S.; Abeygunawardana, C.; Johnson, M. O.; Vanzijl, P. C. M. *J. Magn. Reson. B* **1995**, *108*, 94−98.
(17) Keppel, T. R.; Howard, B. A.; Weis, D. D. *Biochemistry* **2011**, *50*, 8722−8732.
(18) Wales, T. E.; Engen, J. R. *Mass Spectrom. Rev.* **2006**, *25*, 158−170.
(19) Ferguson, P. L.; P, J.; Wilson, D. J.; Dempsey, B.; Lajoie, G.; Shilton, B.; Konermann, L. *Anal. Chem.* **2007**, *79*, 153−160.
(20) Jorgensen, T. J. D.; Gardsvoll, H.; Ploug, M.; Roepstorff, P. *J. Am. Chem. Soc.* **2005**, *127*, 2785−2793.
(21) Hoerner, J. K.; Xiao, H.; Dobo, A.; Kaltashov, I. A. *J. Am. Chem. Soc.* **2004**, *126*, 7709−7717.
(22) Konermann, L.; Pan, J.; Liu, Y.-H. *Chem. Soc. Rev.* **2011**, *40*, 1224−1234.
(23) Rand, K. D.; Lund, F. W.; Amon, S.; Jorgensen, T. J. D. *Int. J. Mass Spectrom.* **2011**, *302*, 110−115.
(24) Zhang, H. M.; Bou-Assaf, G. M.; Emmett, M. R.; Marshall, A. G. *J. Am. Soc. Mass Spectrom.* **2009**, *20*, 520−524.
(25) Dempsey, C. E. *Prog. Nucl. Magn. Reson. Spectrosc.* **2001**, *39*, 135−170.
(26) Marcsisin, S. R.; Engen, J. R. *Anal. Bioanal. Chem.* **2010**, *397*, 967−972.
(27) Raschke, T. M.; Marqusee, S. *Nat. Struct. Biol.* **1997**, *4*, 505−505.
(28) Chamberlain, A. K.; Handel, T. M.; Marqusee, S. *Nat. Struct. Biol.* **1996**, *3*, 782−787.
(29) Hwang, T. L.; van Zijl, P. C. M.; Mori, S. *J. Biomol. NMR* **1998**, *11*, 221−226.
(30) Mori, S.; Abeygunawardana, C.; Berg, J. M.; vanZijl, P. C. M. *J. Am. Chem. Soc.* **1997**, *119*, 6844−6852.
(31) Rob, T.; Wilson, D. J. *J. Am. Soc. Mass Spectrom.* **2009**, *20*, 124−130.
(32) Liuni, P.; Rob, T.; Wilson, D. J. *Rapid Commun. Mass Spectrom.* **2010**, *24*, 315−320.
(33) Brown, L.; Koerner, T.; Horton, J. H.; Oleschuk, R. D. *Lab Chip* **2006**, *6*, 66−73.
(34) Landreh, M.; Astorga-Wells, J.; Johansson, J.; Bergman, T.; Jörnvall, H. *FEBS J.* **2011**, *278*, 3815−3821.
(35) Wang, B.; Oleschuk, R. D.; Petkovich, P. M.; Horton, J. H. *Colloids Surf., B* **2007**, *55*, 107−114.
(36) Pan, J. X.; Han, J.; Borchers, C. H.; Konermann, L. *Anal. Chem.* **2010**, *82*, 8591−8597.
(37) Rand, K. D.; Lund, F. W.; Amon, S.; Jørgensen, T. J. D. *Int. J. Mass Spectrom.* **2011**, *302*, 110−115.
(38) Wilson, D. J.; Konermann, L. *Anal. Chem.* **2003**, *75*, 6408−6414.
(39) Hamuro, Y.; Coales, S. J.; Southern, M. R.; Nemeth-Cawley, J. F.; Stranz, D. D.; Griffin, P. R. *J. Biol. Tech.* **2003**, *14*, 171−82.
(40) Lange, O. F.; Lakomek, N.-A.; FarÃs, C.; Schroeder, G. F.; Walter, K. F. A.; Becker, S.; Meiler, J.; Grubmuller, H.; Griesinger, C.; de Groot, B. L. *Science* **2008**, *320*, 1471−1475.
(41) Bougault, C.; Feng, L. M.; Glushka, J.; Kupce, E.; Prestegard, J. H. *J. Biomol. NMR* **2004**, *28*, 385−390.

(42) Vijay-Kumar, S.; Bugg, C. E.; Cook, W. J. *J. Mol. Biol.* **1987**, *194*, 531−544.
(43) Wang, L. T.; Pan, H.; Smith, D. L. *Mol. Cell. Proteomics* **2002**, *1*, 132−138.
(44) Bai, Y. W.; Sosnick, T. R.; Mayne, L.; Englander, S. W. *Science* **1995**, *269*, 192−197.
(45) Hoang, L.; Bedard, S.; Krishna, M. M. G.; Lin, Y.; Englander, S. W. *Proc. Natl. Acad. Sci. U.S.A.* **2002**, *99*, 12173−12178.
(46) Banci, L.; Bertini, I.; Gray, H. B.; Luchinat, C.; Reddig, T.; Rosato, A.; Turano, P. *Biochemistry* **1997**, *36*, 9867−9877.
(47) Milne, J. S.; Xu, Y. J.; Mayne, L. C.; Englander, S. W. *J. Mol. Biol.* **1999**, *290*, 811−822.
(48) Shumilin, I. A.; Zhao, C.; Bauerle, R.; Kretsinger, R. H. *J. Mol. Biol.* **2002**, *320*, 1147−1156.
(49) Nabuurs, S. M.; van Mierlo, C. P. M *J. Biol. Chem.* **2010**, *285*, 4165−4172.
(50) Moreland, J. L.; Gramada, A; Buzko, O. V.; Zhang, Q.; Bourne, P. E. *BMC Bioinf.* **2005**, 6.